

H₂ emission in the low-ionization structures of the Planetary Nebulae NGC 7009 and NGC 6543

Stavros Akras^{1,2,3*}, Denise R. Gonçalves¹, Gerardo Ramos-Larios⁴, Isabel Aleman⁵

¹Observatório do Valongo, Universidade Federal do Rio de Janeiro, Ladeira Pedro Antonio 43, 20080-090, Rio de Janeiro, Brazil

²Instituto de Matemática, Estatística e Física, Universidade Federal do Rio Grande, Rio Grande 96203-900, Brazil

³Observatório Nacional/MCTIC, Rua Gen. José Cristino, 77, 20921-400, Rio de Janeiro, Brazil

⁴Instituto de Astronomía y Meteorología, CUCEI, Av. Vallarta No. 2602, Col. Arcos Vallarta, CP 44130, Guadalajara, Jalisco, Mexico

⁵Instituto de Física e Química, Universidade Federal de Itajubá, Av. BPS 1303 Pinheirinho, 37500-903 Itajubá, MG, Brazil

Accepted XXX. Received YYY; in original form ZZZ

ABSTRACT

Despite the many studies in the last decades, the low-ionization structures (LISs) of planetary nebulae (PNe) still hold several mysteries. Recent imaging surveys have demonstrated that LISs are composed of molecular gas. Here, we report H₂ emission in the LISs of NGC 7009 and NGC 6543 by means of very deep narrow-band H₂ images taken with NIRI@Gemini. The surface brightness of the H₂ 1-0 S(1) line is estimated to be $(0.46\text{--}2.9)\times 10^{-4}$ erg s⁻¹ cm⁻² sr⁻¹ in NGC 7009 and $(0.29\text{--}0.48)\times 10^{-4}$ erg s⁻¹ cm⁻² sr⁻¹ in NGC 6543, with signal-to-noise ratios of 10-42 and 3-4, respectively. These findings provide further confirmation of hidden H₂ gas in LISs. The emission is discussed in terms of the recent proposed diagnostic diagram $R(\text{H}_2)=\text{H}_2$ 1-0 S(1)/H₂ 2-1 S(1) versus $R(\text{Br}\gamma)=\text{H}_2$ 1-0 S(1)/Br γ , which was suggested to trace the mechanism responsible for the H₂ excitation. Comparing our observations to shock and ultraviolet (UV) molecular excitation models, as well as a number of observations compiled from the literature showed that we cannot conclude for either UV or shocks as the mechanism behind the molecular emission.

Key words: ISM: molecules; (ISM:) photodissociation region (PDR); planetary nebulae: individual: NGC 7009, NGC 6543; Infrared: general

1 INTRODUCTION

Thirty two years have passed since the report of the ‘low-ionization inclusions’ in planetary nebulae (PNe) by Balick (1987). After that pioneering work, several studies have been carried out, using high-quality imagery and spectroscopy, with the aim to unveil the true nature of these microstructures, explore the physical properties that make them differ from the surrounding nebular medium, in terms of the emission line fluxes, and give insights into their formation mechanism (e.g. Balick et al. 1993, 1994, 1998; Hajian et al. 1997).

Since then, several PNe have been found to host these microstructures (e.g. Corradi et al. 1996) and different labels have been given based on their properties: fast low-ionization emission regions (FLIERS, Balick et al. 1993), slow moving low ionization emitting regions (SLOWERS, Perinotto 2000) or bipolar, rotating, episodic jets (BRETs, Lopez et al. 1993,

1995). We will hereafter refer to all of them as low-ionization structures or LISs (see Gonçalves et al. 2001).

Gonçalves et al. (2001) reviewed the kinematic and morphological characteristics of LISs and discussed possible links with various formation models. The authors came to the conclusion that there is no direct connection between LISs and the morphology of PNe, since they appear in all types (round, elliptical, bipolar, or point-symmetric). Various formation models of knots and/or jets are able to explain some of their observable characteristics but not all of them. So far, there is not a general model that can provide an adequate explanation for all the microstructures.

Shock interactions have been proposed as a possible mechanism to explain the enhancement in low-ionization lines like [O I], [N I], [S II], [O II], and [N II] (e.g. Hartigan et al. 1994; Dopita 1997). Running a series of numerical simulations for a high-density knot moving outwards in a less dense medium, Raga et al. (2008) demonstrated that the spectral characteristics of shock-excited or photoionized regions can both be reproduced by changing the local photoionization rate. Low photoionization rate models gener-

* E-mail: stavrosakras@gmail.com

Table 1. Observations log

Filter	λ_c (μm)	$\Delta\lambda$ (μm)	Time ^a (s)	Number of frames	Time ^a (s)	Number of frames
NGC 7009				NGC 6543		
K-cont-1	2.0975	0.0275	100	7	90	7
H ₂ 1-0 S(1)	2.1239	0.0261	100	6	90	7
Brackett γ	2.1686	0.0295	45	5	45	5
H ₂ 2-1 S(1)	2.2465	0.0301	173	17	163	16
K-cont-2	2.2718	0.0352	173	16	163	14

^a Integration time of each individual frame.

ate spectroscopic characteristics similar to shock-excited regions. A crucial parameter to distinguish the mechanisms is the distance between the LISs and the source of ionizing photons, which determines the photoionization rate at the position of the structures (Aleman et al. 2011; Akras & Gonçalves 2016).

Based on Raga’s simulations and spectroscopic data from a sample of PNe with LISs, Gonçalves et al. (2009) argued that the spectra of high-velocity knots can be explained by shocks. A few years later, Akras & Gonçalves (2016) shown that the enhancement of low-ionization lines in knots relative to the surrounding medium is the result of a combination of the ultraviolet (UV) radiation from the central star and shock interactions. However, it is not easy to distinguish the contribution from each mechanisms. On the other hand, there are studies which attribute the enhancement of low-ionization lines in some LISs only to the UV stellar radiation of the central star (e.g. Hajian et al. 1997; Gonçalves 2004; Ali & Dopita 2017). Despite all this effort so far, LISs are still poorly understood.

One of the most intriguing characteristic of LISs is the electronic density (determined from the common diagnostic line ratios), which is systematically lower than or at most equal to the electronic density of the surrounding nebular gas (e.g. Balick et al. 1993; Hajian et al. 1997; Gonçalves et al. 2003, 2009; Monteiro et al. 2013; Akras & Gonçalves 2016; Ali & Dopita 2017). This finding contradicts the formation models of knots in which they are considered more dense than the surrounding nebular gas (e.g. Steffen et al. 2001; Raga et al. 2008). Gonçalves et al. (2009) proposed the scenario that LISs are also made of molecular gas and dust, similarly to the cometary knots of Helix (e.g. Huggins et al. 2002; Meixner et al. 2005; Matsuura et al. 2007, 2009).

Matsuura et al. (2007, 2008) shown that the intensities of the ro-vibrational H₂ lines from the cometary knots of Helix can be explained either by a low-velocity shock of 27 km s⁻¹ or a strong UV stellar radiation field. Interestingly, the latter requires a more luminous central star than the observations indicate i.e. higher local ionization parameter. More detailed simulations by Aleman et al. (2011) have, however, shown that shocks are not needed to explain the observed H₂ surface brightness.

Besides, the cometary of Helix, H₂ emission has also been detected in the cometary knots of the Ring nebula (Speck et al. 2003) and the Dumbbell nebula (Baldridge 2017).

None the less, H₂ emission had not been detected in LISs despite various surveys (e.g. Latter et al. 1995; Kast-

ner et al. 1996; Hora et al. 1999; Guerrero et al. 2000). The main reason for that was the limited spatial resolution and sensitivity of these observations. More sensitive and deeper observations over the last five years have already provided strong evidence as well as the first direct confirmations of H₂ emission associated with LISs in PNe. First, Fang et al. (2015) detected H₂ emission from the northwestern knot of Hu 1-2. Couple of years later, Akras, Gonçalves and Ramos-Larios (2017) succeed to detect the H₂ emission from the LISs in two PNe, K 4-47 and NGC 7662, using very deep narrow-band imagery from the 8 m Gemini North telescope. Fang et al. (2018) reported the detection of H₂ emission from two distant pairs of knots in Hb 12, from a number of randomly distributed knots in the haloes of NGC 6543 and NGC 7009 as well as from the pair of LISs in the ionized region of NGC 7009. Regarding Hb 12, it should be mentioned that despite the H₂ from its distant clumps, strong H₂ 1-0 S(1) emission has also been detected in the centre of the nebula (Dinerstein et al. 1988; Ramsay et al. 1993; Luhman & Rieke 1996), and its origin is pure UV-fluorescence. It should also be noted that H₂ emission detected in the equatorial regions of some bipolar PNe has been unveiled to be fragmented into clumps and filaments (Marquez-Lugo et al. 2013; Machado et al. 2015).

In this paper, we present new deep H₂ narrow-band NIRI@Gemini images for two of the most well-studied PNe, NGC 7009 and NGC 6543. The paper is organized as follows: observations are described in Section 2. In Sections 3 and 4, we present the results of H₂ detection in NGC 7009 and NGC 6543. The mechanisms responsible for the excitation of molecular hydrogen in these structures is discussed in Section 5, and we finish with our conclusions in Section 6.

2 OBSERVATIONS

The observations of NGC 7009 and NGC 6543 were acquired in service mode on 2017 May 10 and June 24 (Program ID: GN-2017A-Q-58, PI: S. Akras) using the Near InfraRed Imager and Spectrometer on the Gemini-North Telescope at Mauna Kea in Hawaii.

The narrow-band filters G0216, G0218 and G0220 were used to isolate the H₂ 1-0 S(1), H₂ 2-1 S(1) and Br γ lines centred at 2.1239, 2.2465 and 2.1686 μm , respectively, as well as the filters G0217 and G2019 centred at 2.0975 and 2.2718 μm to obtain the continuum emission. Due to the targets’ sizes, the f/6 configuration was adopted providing a field of view of 120 arcsec² and pixel size of 0.117 arcsec.

Table 2. Emission-line fluxes for NGC 7009 and NGC 6543, in units of 10^{-15} erg s $^{-1}$ cm $^{-2}$. $R(H_2) = H_2$ 1-0 S(1)/1-2 S(1) and $R(Bry) = H_2$ 1-0 S(1)/Bry. Numbers in parenthesis correspond to the S/Ns. Lower rows give the surface brightness in units of 10^{-4} erg s $^{-1}$ cm $^{-2}$ sr $^{-1}$.

Name	R.A.	Dec.	H ₂ 1-0 S(1)	H ₂ 2-1 S(1)	Bry	$R(H_2)$	$R(Bry)$	Box (arcsec 2)
NGC 7009:								
LIS-E1	21:04:12.486	-11:21:41.903	3.71 (42)	0.38 (19)	2.61 (17)	9.76	1.42	0.583×0.931
			2.91	0.30	2.05			
LIS-E2	21:04:12.743	-11:21:36.836	1.06 (10)	0.13 (5)	2.05 (9)	8.15	0.52	0.932×1.049
			0.46	0.06	0.89			
LIS-W1	21:04:09.029	-11:21:52.942	11.4 (14)	3.26 (8)	28.2 (11)	3.50	0.40	3.965×2.564
			0.48	0.14	1.18			
LIS-W1	21:04:09.029	-11:21:53.175	8.13 (15)	2.39 (10)	16.7 (12)	3.40	0.49	2.682×2.214
			0.58	0.17	1.20			
LIS-W1	21:04:09.009	-11:21:52.933	7.36 (15)	1.98 (7)	13.6 (11)	3.72	0.54	3.382×1.515
			0.61	0.16	1.13			
NGC 6543:								
LIS-SW	17:58:32.103	+66:37:47.725	2.99 (3)	<0.9 ^a	44.8 (7)	>3.32 ^b	0.07	2.020×1.858
			0.34	<0.10 ^a	5.08			
LIS-SW	17:58:32.053	+66:37:47.404	6.03 (3)	<2.08 ^a	86.3 (7)	>2.89 ^b	0.07	3.150×2.760
			0.30	<0.10 ^a	4.22			
LIS-SW	17:58:32.155	+66:37:46.968	1.26 (3)	<0.44 ^a	8.56 (6)	>2.86 ^b	0.15	0.747×2.468
			0.29	<0.10 ^a	1.98			
LIS-NE	17:58:33.800	+66:38:11.717	1.97 (4)	<0.42 ^a	35.1 (7)	>4.69 ^b	0.06	1.723×1.002
			0.49	<0.10 ^a	8.65			

^aThese numbers correspond to the 3σ upper limits. ^bThese numbers correspond to the 3σ lower limits.

Several individual frames, with different exposure times per filter, were obtained in order to increase the signal-to-noise (S/N) ratio. The observing log is summarized in Table 1.

Darks and GCAL flat frames were also obtained for the correction of the thermal emission, dark current and hot pixels. In order to reduce the total time of the observations, the major axis of the targets was oriented in the up-down direction on the detector, which made possible to carry out the dithering across the left-right direction (minor-axis of the nebula) and avoid the additional observations for the sky background. Standard stars (TYC 4413-304-1 and GSPC S813-D) were also observed to flux calibrate the data.

All first frames from each sequence were removed from the reduction/analysis as recommended by Gemini. Before start the reduction process, the PYTHON routines CLEARIR.py and NIRLIN.py¹ were applied to all the frames for the correction of the vertical stripping and the non-linearity of the detector. The reduction of the data was then performed with the GEMINI IRAF² package for NIRI. The routines *Nprepare*, *Nsky*, *Nflat*, *Nreduce* and finally *Imcoadd* were used for each imaging set accordingly.

The estimated surface brightness sensitivity of the H₂ 1-0 S(1), H₂ 2-1 S(1) and Bry images are 2.8×10^{-16} ,

1.3×10^{-16} , and 1.9×10^{-15} erg s $^{-1}$ cm $^{-2}$ arcsec $^{-2}$, respectively for NGC 7009. For NGC 6543, the corresponding sensitivities are 3.1×10^{-16} , 2.4×10^{-16} and 2.3×10^{-15} erg s $^{-1}$ cm $^{-2}$ arcsec $^{-2}$, respectively.

3 H₂ IN NGC 7009

In spite of NGC 7009 being one of the most well-studied PN, only a year ago H₂ emission was reported at the tips of the two jet or jet-like LISs in the ionized region of this nebula (Fang et al. 2018). However, these detections were not supported by a continuum-subtracted image or any H₂ 1-0 S(1) flux measurement, but only by the spatial offset between the H₂ and Bry emission-lines. Therefore, more observations were needed to confirm the results.

Before the undoubted detection of H₂ gas in the LISs of NGC 7009, Phillips et al. (2010) had carried out a detailed analysis of this PN using Infrared Array Camera (IRAC) images (i.e. [3.6], [4.5], [5.8] and [8] μ m) and the available spectra in the ISO and *Spitzer* archives. From the three-colours RGB IRAC image of NGC 7009 (see fig. 1 in Phillips et al. 2010), both LISs (outflow+knots) are displayed with green colour, which corresponds to the emission from the [4.5] band. Sources with enhanced emission at the [4.5] band are usually found close to young stellar objects and attributed to outflows (De Buizer & Vacca 2010), being known as “Green fuzzies” (Chambers et al. 2009). By analysing spectroscopic data of “Green fuzzy” sources, De Buizer & Vacca (2010) argued that H₂ emission is likely the primary emission in the [4.5] band. The same correlation has also been found in the Helix nebula, for which the cometary knots are unam-

¹ CLEARIR.py and NIRLIN.py PYTHON routines were developed and are distributed by Gemini for a preparatory reduction of the data obtained with NIRI and GNIRS, <https://www.gemini.edu/sciops/instruments/niri/>

² IRAF is distributed by the National Optical Astronomy Observatories, which are operated by the Association of Universities for Research in Astronomy, Inc., under cooperative agreement with the National Science Foundation

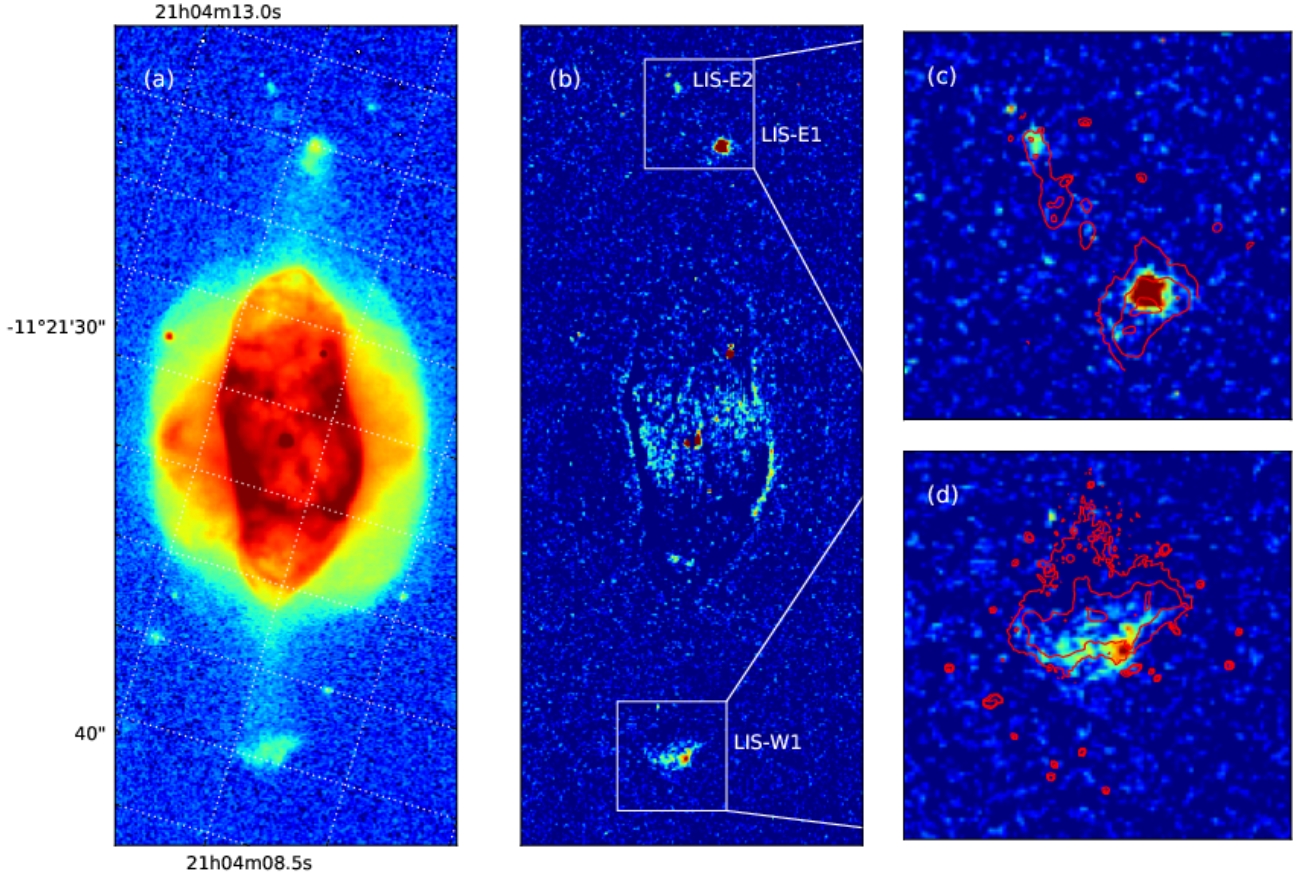


Figure 1. Gemini NIRI images of NGC 7009. LISs are labelled as W1, E1 and E2. H₂ 1-0 S(1) line image (panel a), H₂ 1-0 S(1) continuum-subtracted image (panel b), and H₂ 1-0 S(1) continuum-subtracted images of W1 and E1/E2 LISs overlaid by *HST* [N II] λ 6584 emission contours (panels c and d).

biguously bluer in the [4.5]-[8.0] colour index compared to the nebular gas due to the stronger emission from the [4.5] band dominated by H₂ lines (Hora et al. 1999). Molecular hydrogen lines from the ground rotational state such as 0-0 S(7), 0-0 S(4), and 0-0 S(5) may also contribute to the [5.8] and [8.0] IRAC bands (Hora et al. 2004). The strong IRAC [4.5] emission found in the outflow and knots of NGC 7009 was an indirect indication of possible H₂ emission in these substructures, but a strong contribution from the Br α line at 4.052 μ m could not be ruled out (Phillips et al. 2010).

Our more sensitive and high spatial resolution narrow-band images of NGC 7009 have detected the ro-vibrational H₂ 1-0 S(1) and 2-1 S(1) emission-lines from three substructures, confirming the results from Fang et al. (2018). They are designated E1, E2, and W1 in Figures 1-3. The main body of NGC 7009 is characterized by an ellipsoidal nebula, known as Saturn nebula, with a pair of highly collimated outflows and knots. Both knots are bright in low-ionization lines such as [N II], [O II], [S II], and [O I] (Gonçalves et al. 2003, 2006; Walsh et al. 2018). The E1 and W1 LISs correspond to the K1 and K4 knots in Gonçalves et al. (2003, 2006). There is also a marginal detection of H₂ emission from the main nebula but only spectroscopic follow-up observations can confirm whether it is real or remnant from the continuum subtraction process. It is interesting, though,

that this emission follows the morphology of the outer edge of the ellipsoidal nebula.

The emission line fluxes of the three LISs are listed in Table 2. The H₂ 1-0 S(1) line flux varies from 1.06 to 11.4×10^{-15} erg s⁻¹ cm⁻² with an S/N higher than 10, while the H₂ 2-1 S(1) line flux varies between 0.129 and 3.26×10^{-15} erg s⁻¹ cm⁻² with an S/N higher than 5. The $R(\text{H}_2)=\text{H}_2$ 1-0 S(1)/H₂ 1-2 S(1) line ratio is found to be significantly different between the eastern and western LISs. In particular, the E1 and E2 LISs have $R(\text{H}_2)$ equal to 9.81 and 8.22, respectively, which are approximately three times higher than the value of W1 LIS. Because of the irregular morphology of W1 LIS, we present three estimates of the fluxes obtained from different aperture sizes, and all of them result in very similar $R(\text{H}_2)$ ratio, from 3.40 to 3.72.

Bry emission is also detected in all the three LISs with fluxes between 2.05 and 28.2×10^{-15} erg s⁻¹ cm⁻². The $R(\text{Bry})=\text{H}_2$ 1-0 S(1)/Bry line ratio does not show significant differences among the LISs (see Table 1), and it is comparable with the values derived for the LISs in NGC 7662 (Akras et al. 2017).

A comparison between the H₂ 1-0 S(1) and H₂ 2-1 S(1) lines with the [N II] *Hubble Space Telescope* (*HST*) image at 6584 Å shows a very good match (Figures 1 and 3), with the former being engulfed by the [N II] emission. Figure 2 displays the distribution of the Bry line and its comparison

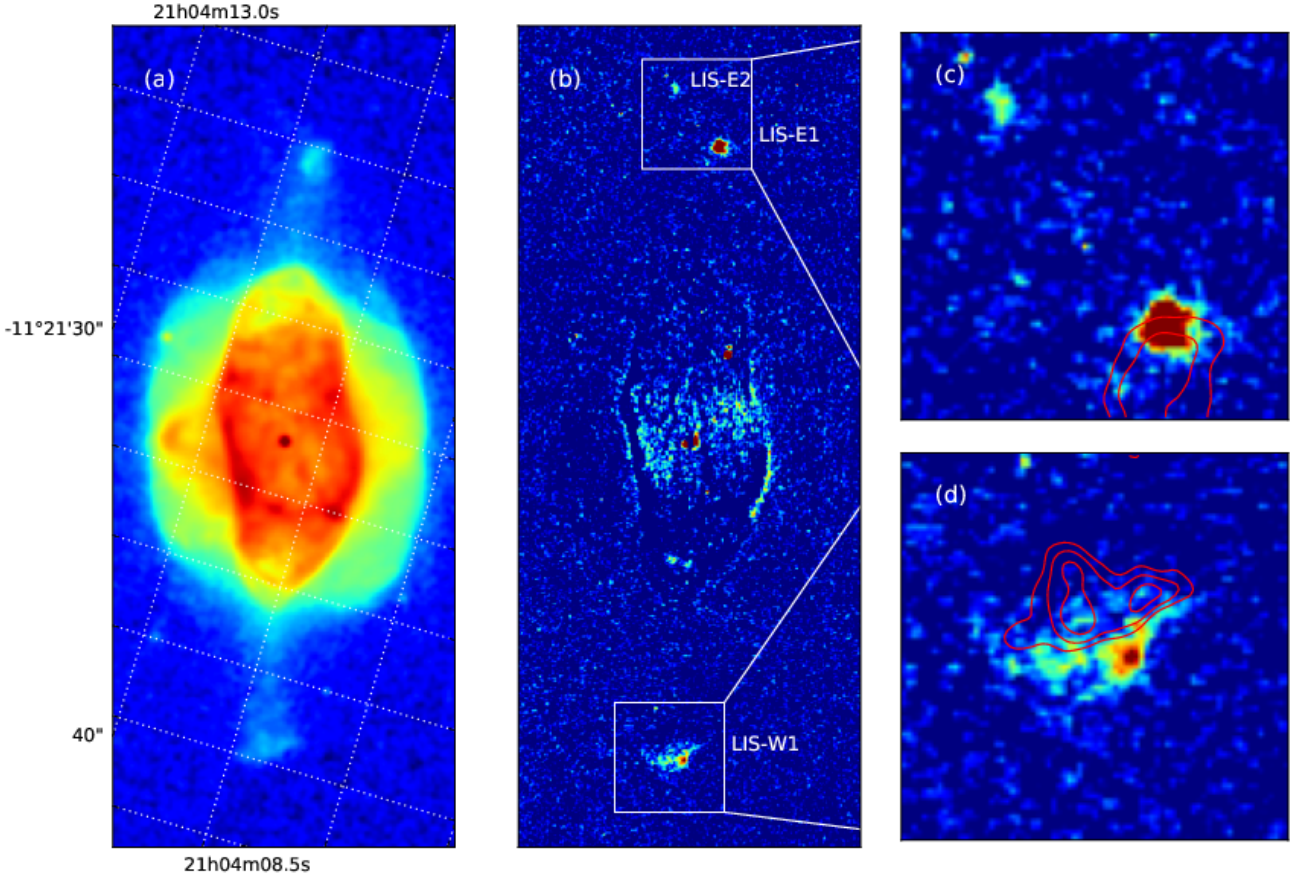


Figure 2. The same as Figure 1. Bry line image (panel a), H_2 1-0 S(1) continuum-subtracted image (panel b), and H_2 1-0 S(1) continuum-subtracted images of W1 and E1/E2 LISs overlaid by Bry emission contours (panels c and d).

with the bright H_2 1-0 S(1) line. The spatial displacement between the Bry and H_2 emissions reported by Fang et al. (2018) is also observed in our data.

Gonçalves et al. (2003, 2006) identified two more LISs, labelled K2 and K3, which lie closer to the central star, but no H_2 emission is detected in these two LISs. The detection of H_2 emission in four more knots distributed in the halo of NGC 7009, at distances higher than 1 arcmin from the central star, has also been reported (Fang et al. 2018).

4 H_2 IN NGC 6543

NGC 6543, the second PN observed with NIRI at the Gemini-North (Program ID:GN-2017A-Q-58), is characterized by a bipolar structure with a pair of condensations and jets bright in low ionization lines (Balick et al. 1994; Balick 2004; Balick & Hajian 2004).

Similar to NGC 7009, halo features in NGC 6543 also appear with green colour in the three-colours RGB IRAC images (fig. 1 and 9 in Hora et al. 2004; Fang et al. 2018). As we have already pointed out, the strong emission from the [4.5] band is attributed to molecular lines that fall within this band (Hora et al. 1999; De Buizer & Vacca 2010). Only last year, Fang and coworkers reported the detection of H_2 emission from the knotty and filamentary halo that surrounds NGC 6543 (Fang et al. 2018).

In contrast to Fang et al.'s (2018) work, the focus of this

work is on the bright ionized bipolar nebula of NGC 6543, also known as the Cat's Eye Nebula, and not on its recombination halo. The narrow-band H_2 1-0 S(1) NIRI image of NGC 6543 is presented in Figure 4. The image is smoothed using a Gaussian function with a radius of 2σ so as we can better illustrate the detection of the emission in the SW and NE LISs. These LISs correspond to the F-F' condensations between the caps and the jets in Miranda & Solf (1992). The H_2 1-0 S(1) line fluxes are estimated between 1.26 and $2.99 \times 10^{-15} \text{ erg s}^{-1} \text{ cm}^{-2}$ with S/N ratio of 3-4 (see also Table 2). Three flux measurements derived from different aperture sizes are given for the SW LIS. The detection of H_2 emission from both LISs of NGC 6543 is reported for the first time. A marginal detection of H_2 emission at the edges of the bipolar lobes, labelled as "caps" in Balick et al. (1994) and D-D' in Miranda & Solf (1992) can also be seen in Figure 4, but deep follow-up spectroscopic observations are necessary to confirm this emission. The H_2 2-1 S(1) line at $2.24 \mu\text{m}$ is not detected in NGC 6543, but we obtained upper limits for its emission, which yields lower limits for the $R(H_2)$ ratio between 2.9 and 4.7 (Table 2).

Both LISs in NGC 6543 are detected in the Bry line (Figure 5) with fluxes between 8.56 and $86.3 \times 10^{-15} \text{ erg s}^{-1} \text{ cm}^{-2}$ and S/N ratio of 6-7 (see Table 2). Their $R(\text{Bry})$ ratios have been estimated between 0.06 and 0.15, close to the values calculated for some LISs in NGC 7662 (Akra et al. 2017). From Figure 5, it can also be seen that a diffuse

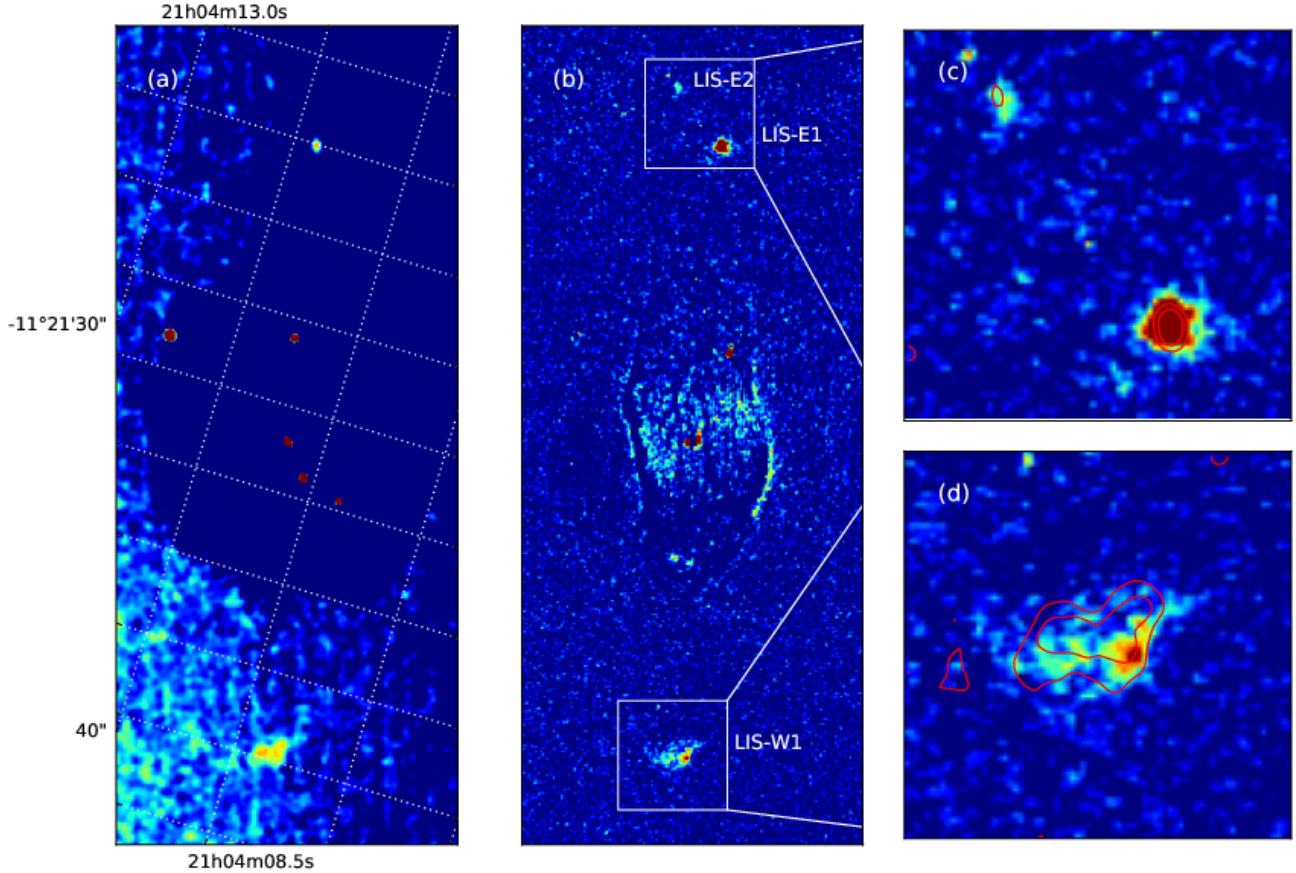


Figure 3. The same as Figure 1. H₂ 2-1 S(1) continuum-subtracted image (panel a), H₂ 1-0 S(1) continuum-subtracted image (panel b), and H₂ 1-0 S(1) continuum-subtracted images of W1 and E1/E2 LISs overlaid by H₂ 2-1 S(1) emission contours (panels c and d).

emission from the nebula itself surrounds the LISs and it may contribute to the Br γ fluxes. This additional emission may be responsible for the very low $R(\text{Br}\gamma)$ ratios found in the LISs.

A comparison of our H₂ 1-0 S(1) image with the *HST* [N II] $\lambda 6584$ image show a strong correlation (Figure 4). Similarly to NGC 7009, H₂ emission is engulfed by the more extended [N II] emission. Comparison of the spatial distribution in H₂ and Br γ emission-lines illustrates an offset between the two emissions as in NGC 7009.

5 MOLECULAR HYDROGEN EXCITATION

The mechanisms to populate the H₂ (v, J) = (1,3) and (2,3) rovibrational levels, whose decay yield the emission in the 1-0 S(1) and 2-1 S(1) line, respectively, may be dominated by UV pumping or collisions with gas particles, depending on the local physical conditions (see [Aleman & Gruenwald 2011](#), and references therein). For these levels, direct radiative excitation and de-excitation are forbidden via dipole transitions, but allowed by electric quadrupole. The latter has low probability of occurrence, but is the decay mechanism that produces the lines we observe. Formation pumping is also possible, but it is not an important mechanism for those levels in PNe conditions.

Early works on H₂ excitation in PNe (e.g. [Beckwith et al. 1980](#)) suggested the $R(\text{H}_2)$ ratio as a diagnostic for

the molecular excitation mechanism. $R(\text{H}_2) \sim 2$ would indicate that H₂ is excited by UV radiation, while $R(\text{H}_2) > 4$ would point out to H₂ gas excited by collisions with gas particles in shock regions. This inference was based on the sets of models available for UV excitation (e.g. [Black & Dalgarno 1976](#); [Black 1978](#); [Shull 1978](#)), and for shocks ([Kwan et al. 1977](#); [Shull & Hollenbach 1978](#)). [Sternberg & Dalgarno \(1989\)](#) showed, however, that the real picture was not that simple. In certain conditions, such as high-density gas irradiated by UV, collisional excitation can dominate the level excitation and give $R(\text{H}_2)$ ratios that resemble those of a thermalized shock-heated gas.

[Marquez-Lugo et al. \(2015\)](#) proposed as diagnostic for UV- and shock-excited H₂ gas in PNe a plot between the $R(\text{H}_2)$ and $R(\text{Br}\gamma)$ line ratios. Yet, these two line ratios are not enough to argue for the excitation mechanism of molecular hydrogen. For a better diagnostic analysis, it is necessary to study the H₂ level population of more levels, having in mind that all the mechanisms may compete in importance and that the dominant mechanism may vary for different levels and in different physical conditions ([Aleman & Gruenwald 2011](#)). Excitation diagrams are helpful tools to determine the excitation mechanism of H₂ (e.g., [Hora et al. 1999](#); [Lumsden et al. 2001](#)). However, for narrow-band imaging studies like ours, it is not feasible to measure several lines and construct such diagrams. As we can derive the $R(\text{H}_2)$ and $R(\text{Br}\gamma)$ ratios from our observations, we construct

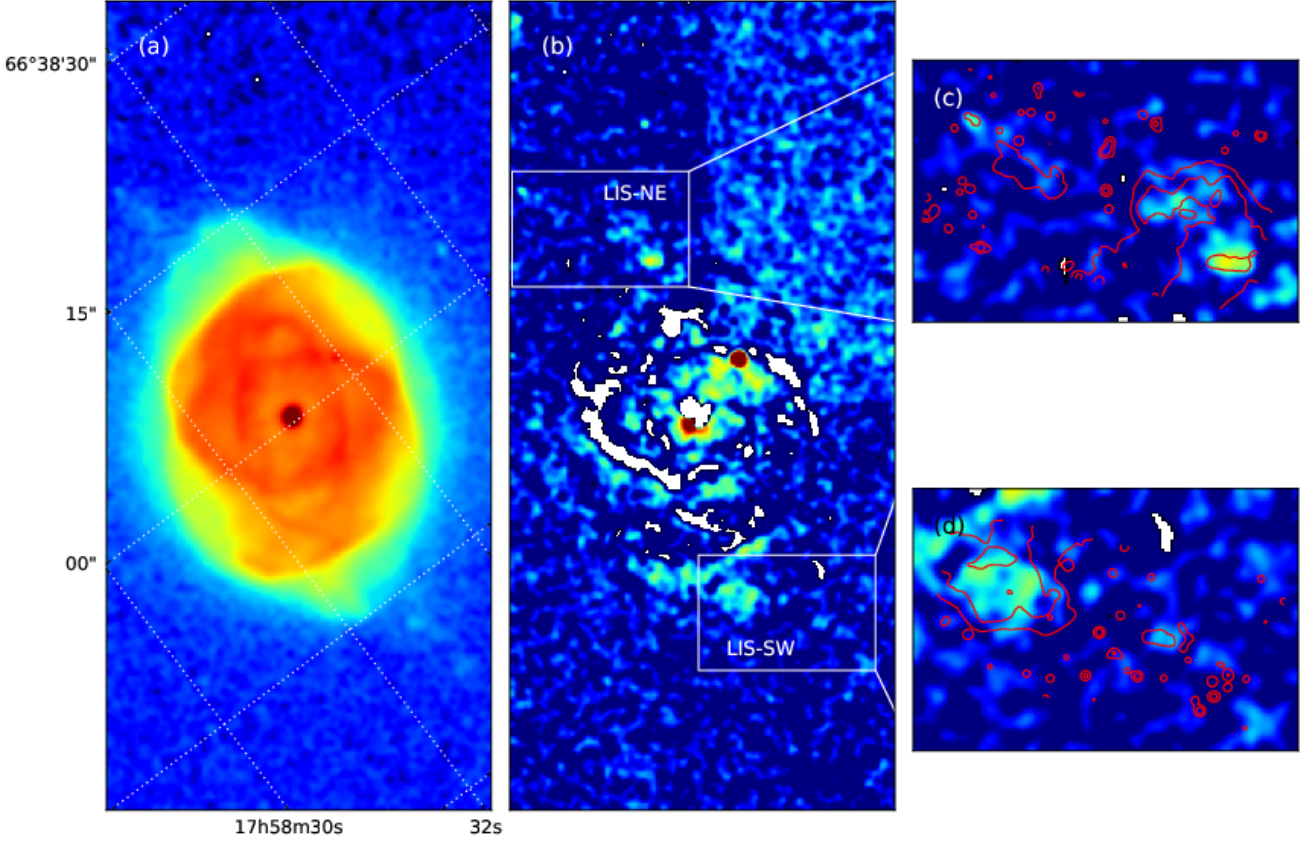


Figure 4. Gemini NIRI imaging of NGC 6543. The pairs of LISs are labelled as SW and NE. H_2 1-0 S(1) line image (panels a), H_2 1-0 S(1) continuum-subtracted image smoothed using a Gaussian function with a radius of 2σ (panel b), and H_2 1-0 S(1) continuum-subtracted images of SW and NE LISs overlaid by *HST* [N II] $\lambda 6584$ emission contours (panels c and d).

the diagnostic diagram as suggested by [Marquez-Lugo et al. \(2015\)](#) to make a preliminary assessment of which excitation mechanism dominates the H_2 level population in LISs. Follow-up spectroscopy studies will be necessary in order to construct more conclusive diagnostic diagrams.

Our $R(H_2)$ vs. $R(Br\gamma)$ diagnostic diagram is shown in Figure 6. In the top panel, we show pre-PNe (orange circles), PNe (blue circles), and candidates PNe (gray circles) gathered from the literature ([Geballe et al. 1991](#); [Aspin et al. 1993](#); [Vicini et al. 1999](#); [Hora et al. 1999](#); [Lumsden et al. 2001](#); [García-Hernández et al. 2002](#); [Davis et al. 2003](#); [Kelly & Hrivnak 2005](#); [Likkell et al. 2006](#); [Ramos-Larios et al. 2008](#); [Gledhill & Forde 2015](#); [Marquez-Lugo et al. 2015](#); [Jones et al. 2018](#)). Model predictions of the $R(H_2)$ ratio obtained from UV irradiated cloud models (photodissociation regions; [Sternberg & Dalgarno 1989](#); [Burton et al. 1990](#)) and shock models ([Smith 1995](#); [Novikov & Smith 2018](#)) are indicated as red and green vertical stripes, respectively.

From a quick observation of the diagnostic diagram, it can be seen that there is a trend between $R(H_2)$ and $R(Br\gamma)$ line ratios, both increasing from the lower right to the upper left corner. This behaviour was attributed to the transition from UV-dominated regions (left-hand side) to shock-dominated regions (right-hand side) ([Marquez-Lugo et al. 2015](#)). But, according to the shocks and UV-irradiated cloud

models, both mechanisms can provide a reasonable explanation for the observable range of $R(H_2)$ values (~ 2 -45).

Note that all but three pre-PNe exhibit $R(Br\gamma) > 1$, while PNe cover the whole range of $R(Br\gamma)$ line ratio from 0.01 up to 100. On the other hand, both PN and pre-PNe shows the same range of $R(H_2)$ from ~ 2 up to ~ 20 (Figure 6). The high $R(H_2)$ found in pre-PNe (or some PNe) indicates that the emission is thermalized, while for those with low $R(H_2)$ the H_2 emission is non-thermal. These findings are consistent with the conclusions of [Davis et al. \(2003\)](#) that shocks may play an important role in the molecular gas excitation of pre-PNe and PNe (see also [Akras et al. 2017](#); [Akras & Gonçalves 2016](#)). However, it is not possible to trace and disentangle the contribution of each excitation mechanism (UV fluorescence or shocks), with this diagnostic diagram.

Two more sets of models, one for PNe ([Aleman & Gruenewald 2011](#)) and one for the Helix nebula cometary knots ([Aleman et al. 2011](#)) are also presented. Both sets correspond to self-consistent photoionization plus photodissociation region models, with the former corresponding to uniform density PNe, while the latter models were specifically developed to simulate one cometary knot (dense clump) subject to different conditions inside the Helix nebula. It is worth mentioning that for the three cometary knot models with $R(Br\gamma) \geq 2$, the distance from the central source varies and the model with the largest distance predicts highest ra-

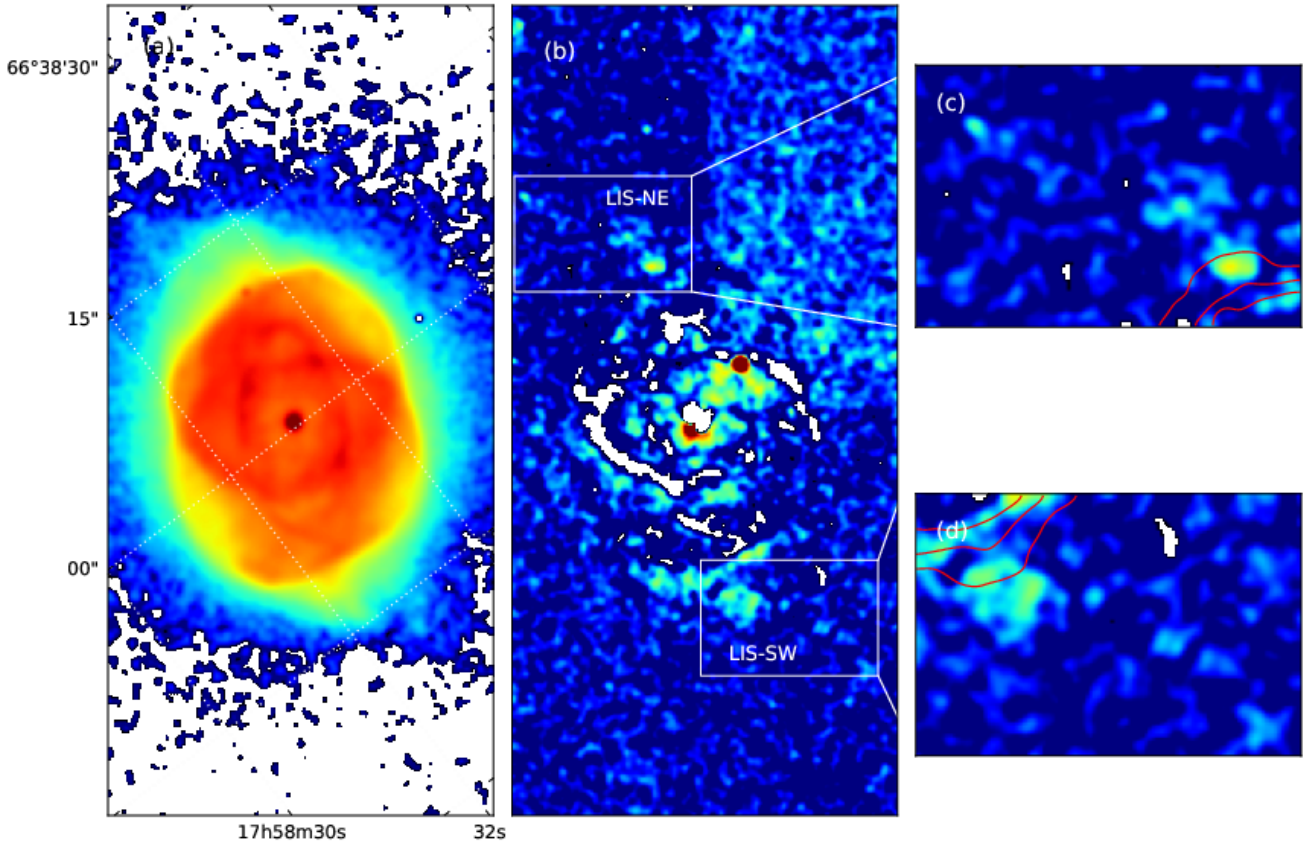


Figure 5. The same as Figure 4. Bry line image (panel a), H₂ 1-0 S(1) continuum-subtracted image smoothed using a Gaussian function with a radius of 2σ (panel b), and H₂ 1-0 S(1) continuum-subtracted images of SW and NE LISs overlaid by Bry emission contours (panels c and d).

tio. The importance of the distance between the dense knot and the central ionization source becomes clear from these models, as discussed in [Aleman & Gruenwald \(2011\)](#), [Akras & Gonçalves \(2016\)](#) and [Akras et al. \(2017\)](#).

The $R(\text{H}_2)$ and $R(\text{Bry})$ ratios of the LISs in NGC 7009 and NGC 6543 obtained in this work as well as those from NGC 7662 and K 4-47 published in [Akras et al. \(2017\)](#) are shown in the bottom panel of Figure 6. A few other measurements obtained for PNe knots are also added in the plot. Studies of the H₂ emission from the PN Hb 12 (green diamonds; [Dinerstein et al. 1988](#), [Ramsay et al. 1993](#), [Luhman & Rieke 1996](#)) are also included in order to show the $R(\text{H}_2)$ and $R(\text{Bry})$ ratios for a molecular gas excited by UV stellar radiation. The $R(\text{H}_2)$ ratio of the K1 cometary knot in Helix determined by [Matsuura et al. \(2007\)](#) is indicated with a cyan diamond. Bry emission is not detected in this knot and a lower limit is provided for the $R(\text{Bry})$, assuming as upper limit intensity that of the marginally detected H₂ 2-1 S(2) line at $2.154\ \mu\text{m}$ (see Table 2 in [Matsuura et al. 2007](#)). The H₂ excitation diagram of the K1 Helix’s knot indicate a thermal origin for its H₂ emission and the dominant mechanism for the excitation of molecular hydrogen is UV-fluorescence pumping, rather than shocks ([O’Dell et al. 2000](#); [Matsuura et al. 2007](#); [Aleman et al. 2011](#); [Andriantsaralaza et al. 2020](#)). We also included measurements made for a diffuse region and a knot in Dumbbell by [Baldridge \(2017\)](#).

The comparable rotational and vibrational excitation temperatures inferred from a few lines indicates a thermal origin for the H₂ emission in Dumbbell nebula.

For NGC 7009, the $R(\text{H}_2)$ ratios of LISs are determined ~ 3.5 for the western LIS and around 9 for the eastern LISs. This difference in the $R(\text{H}_2)$ ratio between the western and eastern LISs is attributed to the potential variation in the incident radiation field at their positions and/or in their column densities ([Sternberg & Dalgarno 1989](#); [Burton et al. 1990](#); [Aleman et al. 2011](#)).

The high $R(\text{H}_2)$ ratios of the eastern LISs (between 8 and 10) indicate a thermal origin and the excitation mechanism can be either shock collisions or thermalized UV-pumping in a warm and high density ($>10^5\ \text{cm}^{-3}$) H₂ gas (e.g. [Sternberg & Dalgarno 1989](#); [Burton et al. 1990](#)). As discussed above, for such values, it is not possible to disentangle the two mechanisms only from the $R(\text{H}_2)$ ratio. The values of $R(\text{H}_2)$ for the eastern LISs are comparable with those measured for two cometary knots in Helix and Dumbbell, and those in K 4-47 (Figure 6). In K 4-47, its H₂ emission is attributed to a thermalized shock-heated gas because of the high expansion velocities of the LISs ($>100\ \text{km s}^{-1}$; [Corradi et al. 2000](#)) and high $R(\text{H}_2)$ ratio ([Akras et al. 2017](#)). Although, thermal emission from pumped-H₂ molecules in warm and dense gas cannot be rule out. The western LIS exhibits $R(\text{H}_2)\sim 3$, which is indicative of UV radiation deter-

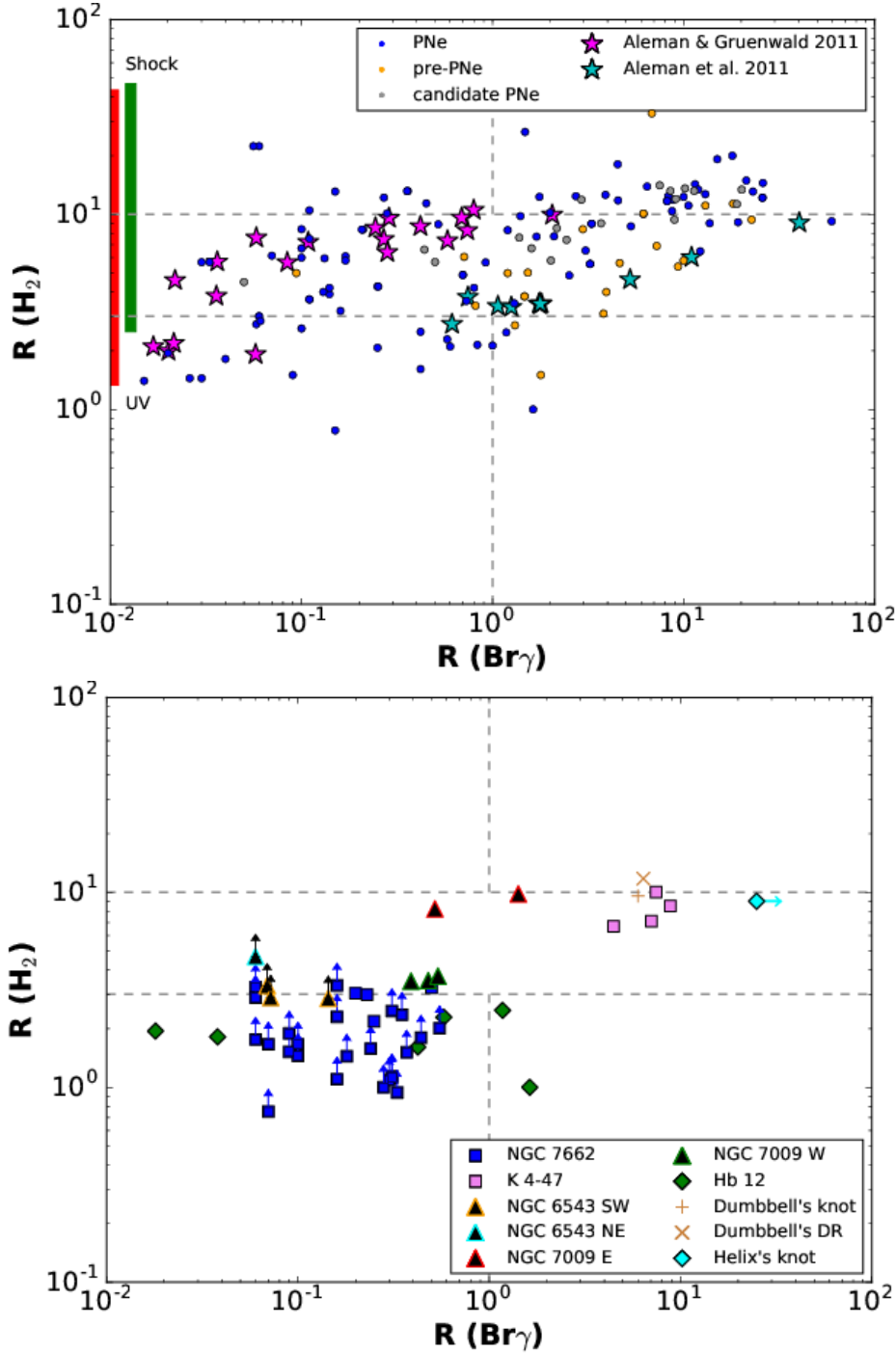


Figure 6. Molecular hydrogen line ratio diagnostic diagram. Top panel: $R(H_2)$ vs. $R(Br\gamma)$ diagram for pre-PNe (orange circles), PNe (blue circles), and candidate PNe (gray circles) from the literature, theoretical predictions from UV models (pink/cyan stars and red vertical strip) and shock models (green vertical strip). Bottom panel: $R(H_2)$ vs. $R(Br\gamma)$ diagram for LISs in NGC 7009, NGC 6543, NGC 7662, and K 4-47 PNe, as well as Dumbbell's knot and nebular diffuse region, and Hb 12's central region (see the text for details). The horizontal dashed lines correspond the typical values for non-thermal (~ 3) and thermal emission (~ 10). The vertical dashed line indicates the border ($R(Br\gamma)=1$) between sources brighter in $Br\gamma$ (left-hand part) and brighter in H_2 1-0.

mining the H_2 level population. This ratio is comparable to the values found for Hb 12.

A further comparison between the observed H_2 1-0 S(1) and 2-1 S(1) emission-lines intensities and the theoretical predictions from photodissociation region (PDR) models (see Table 5 in [Burton et al. 1990](#)) shows a very good agree-

ment for high-density models. Models with densities of 10^5 and 10^6 cm^{-3} provide surface brightness close to our observed values for the W1 and E1 LISs, respectively. The gas density difference indicates that the collisional deexcitation of pumped- H_2 is more efficient in E1 than in W1, resulting

in more populated lower vibrational states and thus higher $R(\text{H}_2)$ ratio.

Recall that long-slit low-resolution spectroscopy of NGC 7009 has shown that E1 and W1 LISs are also characterized by significantly different optical line ratios (Gonçalves et al. 2003, 2006). Based on 3D photoionization modelling, Gonçalves et al. (2006) demonstrated that two models with different optical depths between the LISs and the central star (or in other words altering the intensity of the ionising field of the central star at the distance of each LIS) are needed in order to reproduce their emission line fluxes. There is no clear reason why the optical depth or the photoionization rate between the eastern and western LISs should be different, given that both are located at approximately the same projected distance from the central star. Hence, the density of the gas in the LISs is more likely responsible for the divergences found in the line ratios.

For the pair of LISs (NE and SW) in NGC 6543, we determine $R(\text{Br}\gamma)$ and lower limits for $R(\text{H}_2)$. With the current data available, we cannot trace the excitation mechanism of the molecular gas in NGC 6543's LISs and spectroscopic follow-up observations are needed. UV-fluorescence emission (Black & van Dishoeck 1987; Sternberg & Dalgarno 1989; Burton et al. 1990) as well as thermal H_2 emission from shock-heated gas (Hollenbach & McKee 1989; Burton et al. 1992; Smith 1995; Novikov & Smith 2018) can explain the values obtained for the LISs in this nebula (Figure 6).

Besides the detection of H_2 emission in the LISs of NGC 6543, Fang et al. (2018) also reported the detection of H_2 emission from several clumpy structures in the halo of the PN. Because of the strong optical $[\text{S II}]$ and $[\text{N II}]$ emission-lines detected in these structures, it was claimed that H_2 gas was shock-excited. However, strong $[\text{S II}]$ and $[\text{N II}]$ lines are not necessarily indicative of a shock-heated gas in PNe Akras et al. (2020).

6 CONCLUSIONS

We presented new very deep narrow-band H_2 1-0 S(1) and H_2 2-1 S(1) images of NGC 7009, and H_2 1-0 S(1) image of NGC 6543. H_2 emission was detected from the low-ionization structures in both PNe. The surface brightness of the H_2 1-0 line was estimated between 0.46 and $2.9 \times 10^{-4} \text{ erg s}^{-1} \text{ cm}^{-2} \text{ sr}^{-1}$ for the LISs in NGC 7009 and between 0.29 and $0.48 \times 10^{-4} \text{ erg s}^{-1} \text{ cm}^{-2} \text{ sr}^{-1}$ for the LISs in NGC 6543, with S/N ratios between 10 and 42, and between 3 and 4, respectively. This findings increased the number of LISs with H_2 from four to six, further supporting the scenario that LISs are dense microstructures embedded in PNe, partially consisting of molecular gas.

Scrutinizing the $R(\text{H}_2)$ and $R(\text{Br}\gamma)$ diagnostic diagram, we concluded that the positive trend does not indicate a smooth transition from UV-fluorescent-dominated regions to shock-dominated regions. Based on the theoretical predictions from shock and UV-irradiated cloud models, both mechanisms are able to produce either low or high ratios. Therefore, both mechanisms are important in PNe and they contribute to the molecular hydrogen excitation. However, it is not feasible to trace the mechanism from this diagnostic diagram.

Regarding the NGC 7009, the high $R(\text{H}_2)$ ratios (~ 8 -

10) derived from the eastern LISs were attributed either to a warm and dense gas with thermally populated states or to a thermalized shock-heated gas, whilst the low $R(\text{H}_2)$ and $R(\text{Br}\gamma)$ line ratios determined for the western LIS imply a non-thermal UV-fluorescence H_2 emission from a low-density gas.

On the other hand, the no detection of H_2 2-1 emission from the LISs of NGC 6543 and the lower limit values obtained for $R(\text{H}_2)$ ratio did not allow us to trace the origin of its emission. Radiative UV-fluorescence emission is more likely responsible for the excitation of H_2 gas, but shocks cannot be ruled out.

Overall, these new detections further confirmed the presence of molecular gas in high density, LISs in PNe. Although, a systematic H_2 imaging and spectroscopic survey of PNe with LISs is required in order to understand how the molecular hydrogen was formed or how it survived from the intense UV radiation and what is its dominant excitation mechanism.

ACKNOWLEDGEMENTS

The authors would like to thank the anonymous referee for his/her thorough revision of the paper and his/her constructive comments and suggestions that improved the manuscript. SA acknowledges support from the Brazilian agencies CNPq (grant 454794/2015-0) and CAPES (PNPD fellowship). DRG is partially supported by CNPq grants 304184/2016-0 and 428330/2018-5. GR-L acknowledges support from CONACYT (Mexico). IA acknowledges the support of CAPES, Ministry of Education, Brazil, through a PNPd fellowship. The observations we report here were obtained at the Gemini Observatory (processed using the Gemini IRAF package and Gemini-PYTHON), which is operated by the Association of Universities for Research in Astronomy, Inc., under a cooperative agreement with the NSF on behalf of the Gemini partnership: the National Science Foundation (United States), the National Research Council (Canada), CONICYT (Chile), the Australian Research Council (Australia), Ministério da Ciência, Tecnologia e Inovação (Brazil), and Ministerio de Ciencia, Tecnología e Innovación Productiva (Argentina). This research is also based on observations made with the NASA/ESA *HST*, and obtained from the Hubble Legacy Archive, which is a collaboration between the Space Telescope Science Institute (STScI/NASA), the Space Telescope European Coordinating Facility (ST-ECF/ESA), and the Canadian Astronomy Data Centre (CADC/NRC/CSA).

REFERENCES

- Akras S., Gonçalves D. R., 2016, *MNRAS*, **455**, 930
- Akras S., Gonçalves D. R., Ramos-Larios G., 2017, *MNRAS*, **465**, 1289
- Akras S., Monteiro H., Aleman I., Farias M. A. F., May D., Pereira C. B., 2020, *MNRAS*, (arXiv:2002.12380)
- Aleman I., Gruenwald R., 2011, *A&A*, **528**, A74
- Aleman I., Zijlstra A. A., Matsuura M., Gruenwald R., Kimura R. K., 2011, *MNRAS*, **416**, 790
- Ali A., Dopita M. A., 2017, *Publ. Astron. Soc. Australia*, **34**, e036

- Andriantsaralaza M., Zijlstra A., Avison A., 2020, *MNRAS*, **491**, 758
- Aspin C., et al., 1993, *A&A*, **278**, 255
- Baldrige S. P., 2017, PhD thesis, University of Missouri - Columbia
- Balick B., 1987, *AJ*, **94**, 671
- Balick B., 2004, *AJ*, **127**, 2262
- Balick B., Hajian A. R., 2004, *AJ*, **127**, 2269
- Balick B., Rugers M., Terzian Y., Chengalur J. N., 1993, *ApJ*, **411**, 778
- Balick B., Perinotto M., Maccioni A., Terzian Y., Hajian A., 1994, *ApJ*, **424**, 800
- Balick B., Alexander J., Hajian A. R., Terzian Y., Perinotto M., Patriarchi P., 1998, *AJ*, **116**, 360
- Beckwith S., Neugebauer G., Becklin E. E., Matthews K., Persson S. E., 1980, *AJ*, **85**, 886
- Black J. H., 1978, *ApJ*, **222**, 125
- Black J. H., Dalgarno A., 1976, *ApJ*, **203**, 132
- Black J. H., van Dishoeck E. F., 1987, *ApJ*, **322**, 412
- Burton M. G., Hollenbach D. J., Tielens A. G. G. M., 1990, *ApJ*, **365**, 620
- Burton M. G., Hollenbach D. J., Tielens A. G. G., 1992, *ApJ*, **399**, 563
- Chambers E. T., Jackson J. M., Rathborne J. M., Simon R., 2009, *ApJS*, **181**, 360
- Corradi R. L. M., Manso R., Mampaso A., Schwarz H. E., 1996, *A&A*, **313**, 913
- Corradi R. L. M., Gonçalves D. R., Villaver E., Mampaso A., Perinotto M., Schwarz H. E., Zanin C., 2000, *ApJ*, **535**, 823
- Davis C. J., Smith M. D., Stern L., Kerr T. H., Chiar J. E., 2003, *MNRAS*, **344**, 262
- De Buizer J. M., Vacca W. D., 2010, *AJ*, **140**, 196
- Dinerstein H. L., Lester D. F., Carr J. S., Harvey P. M., 1988, *ApJ*, **327**, L27
- Dopita M. A., 1997, *ApJ*, **485**, L41
- Fang X., Guerrero M. A., Miranda L. F., Riera A., Velázquez P. F., Raga A. C., 2015, *MNRAS*, **452**, 2445
- Fang X., Zhang Y., Kwok S., Hsia C.-H., Chau W., Ramos-Larios G., Guerrero M. A., 2018, *ApJ*, **859**, 92
- García-Hernández D. A., Manchado A., García-Lario P., Domínguez-Tagle C., Conway G. M., Prada F., 2002, *A&A*, **387**, 955
- Geballe T. R., Burton M. G., Isaacman R., 1991, *MNRAS*, **253**, 75
- Gledhill T. M., Forde K. P., 2015, *MNRAS*, **447**, 1080
- Gonçalves D. R., 2004, in Meixner M., Kastner J. H., Balick B., Soker N., eds, *Astronomical Society of the Pacific Conference Series Vol. 313, Asymmetrical Planetary Nebulae III: Winds, Structure and the Thunderbird*. p. 216 ([arXiv:astro-ph/0312527](https://arxiv.org/abs/astro-ph/0312527))
- Gonçalves D. R., Corradi R. L. M., Mampaso A., 2001, *ApJ*, **547**, 302
- Gonçalves D. R., Corradi R. L. M., Mampaso A., Perinotto M., 2003, *ApJ*, **597**, 975
- Gonçalves D. R., Ercolano B., Carnero A., Mampaso A., Corradi R. L. M., 2006, *MNRAS*, **365**, 1039
- Gonçalves D. R., Mampaso A., Corradi R. L. M., Quireza C., 2009, *MNRAS*, **398**, 2166
- Guerrero M. A., Villaver E., Manchado A., García-Lario P., Prada F., 2000, *ApJS*, **127**, 125
- Hajian A. R., Balick B., Terzian Y., Perinotto M., 1997, *ApJ*, **487**, 304
- Hartigan P., Morse J. A., Raymond J., 1994, *ApJ*, **436**, 125
- Hollenbach D., McKee C. F., 1989, *ApJ*, **342**, 306
- Hora J. L., Latter W. B., Deutsch L. K., 1999, *ApJS*, **124**, 195
- Hora J. L., Latter W. B., Allen L. E., Marengo M., Deutsch L. K., Pipher J. L., 2004, *ApJS*, **154**, 296
- Huggins P. J., Forveille T., Bachiller R., Cox P., Ageorges N., Walsh J. R., 2002, *ApJ*, **573**, L55
- Jones A. M., Gledhill T. M., Froebrich D., Smith M. D., 2018, *MNRAS*, **480**, 1563
- Kastner J. H., Weintraub D. A., Gatley I., Merrill K. M., Probst R. G., 1996, *ApJ*, **462**, 777
- Kelly D. M., Hrivnak B. J., 2005, *ApJ*, **629**, 1040
- Kwan J. H., Gatley I., Merrill K. M., Probst R., Weintraub D. A., 1977, *ApJ*, **216**, 713
- Latter W. B., Kelly D. M., Hora J. L., Deutsch L. K., 1995, *ApJS*, **100**, 159
- Likkel L., Dinerstein H. L., Lester D. F., Kindt A., Bartig K., 2006, *AJ*, **131**, 1515
- Lopez J. A., Meaburn J., Palmer J. W., 1993, *ApJ*, **415**, L135
- Lopez J. A., Vazquez R., Rodriguez L. F., 1995, *ApJ*, **455**, L63
- Luhman K. L., Rieke G. H., 1996, *ApJ*, **461**, 298
- Lumsden S. L., Puxley P. J., Hoare M. G., 2001, *MNRAS*, **328**, 419
- Manchado A., Stanghellini L., Villaver E., García-Segura G., Shaw R. A., García-Hernández D. A., 2015, *ApJ*, **808**, 115
- Marquez-Lugo R. A., Ramos-Larios G., Guerrero M. A., Vázquez R., 2013, *MNRAS*, **429**, 973
- Marquez-Lugo R. A., Guerrero M. A., Ramos-Larios G., Miranda L. F., 2015, *MNRAS*, **453**, 1888
- Matsuura M., et al., 2007, *MNRAS*, **382**, 1447
- Matsuura M., et al., 2008, *The Messenger*, **132**, 37
- Matsuura M., et al., 2009, *ApJ*, **700**, 1067
- Meixner M., McCullough P., Hartman J., Son M., Speck A., 2005, *AJ*, **130**, 1784
- Miranda L. F., Solf J., 1992, *A&A*, **260**, 397
- Monteiro H., Gonçalves D. R., Leal-Ferreira M. L., Corradi R. L. M., 2013, *A&A*, **560**, A102
- Novikov I. D., Smith M. D., 2018, *MNRAS*, **480**, 75
- O'Dell C. R., Henney W. J., Burkert A., 2000, *AJ*, **119**, 2910
- Perinotto M., 2000, *Ap&SS*, **274**, 205
- Phillips J. P., Cuesta L. C., Ramos-Larios G., 2010, *MNRAS*, **409**, 881
- Raga A. C., Riera A., Mellema G., Esquivel A., Velázquez P. F., 2008, *A&A*, **489**, 1141
- Ramos-Larios G., Guerrero M. A., Miranda L. F., 2008, *AJ*, **135**, 1441
- Ramsay S. K., Chrysostomou A., Geballe T. R., Brand P. W. J. L., Mountain M., 1993, *MNRAS*, **263**, 695
- Shull J. M., 1978, *ApJ*, **219**, 877
- Shull J. M., Hollenbach D. J., 1978, *ApJ*, **220**, 525
- Smith M. D., 1995, *A&A*, **296**, 789
- Speck A. K., Meixner M., Jacoby G. H., Knezek P. M., 2003, *PASP*, **115**, 170
- Steffen W., López J. A., Lim A., 2001, *ApJ*, **556**, 823
- Sternberg A., Dalgarno A., 1989, *ApJ*, **338**, 197
- Vicini B., Natta A., Marconi A., Testi L., Hollenbach D., Draine B. T., 1999, *A&A*, **342**, 823
- Walsh J. R., et al., 2018, *A&A*, **620**, A169

This paper has been typeset from a \LaTeX file prepared by the author.